EAM
Environmental and Materials
EAM 1(1): 8–19
ISSN 3025-0277

Preparation of boron-doped diamond microelectrodes to determine the distribution size of platinum nanoparticles using current transient method

Aliyah [1], Reza Rizqi Nurhidayat [1], Afiten Rahmin Sanjaya [1], Rahmat Wibowo [1], Yasuaki Einaga[2], Endang Saepudin [1], and Tribidasari Anggraningrum Ivandini [1*]

[1] Department of Chemistry, Faculty of Mathematics and Science, University of Indonesia; Campus UI Depok, Jakarta 16424, Indonesia.
[2] Department of Chemistry, Keio University; 3-14-1 Hiyoshi, 223-8522 Yokohama, Japan.
* Correspondence: ivandini.tri@sci.ui.ac.id

Received Date: May 30, 2023 Revised Date: June 22, 2023 Accepted Date: June 22, 2023

Abstract
Boron-doped diamond (BDD) microelectrodes were prepared to investigate the correlation of hydrazine oxidation current responses with Pt nanoparticle (Pt NP) size distribution. The BDD film was grown on the surface of a tungsten needle with a diameter of 25 µm. An average particle size of around 5 µm BDD crystalline was successfully synthesized using a microwave plasma-assisted chemical vapor deposition technique. The Raman spectrum confirmed the presence of diamond formation as indicated by peaks corresponding to C-C sp^3 bonds, while X-ray photoelectron spectroscopy spectrum showed the presence of C-H and C-OH bonds on the surface of the BDD microelectrode. Meanwhile the Pt nanoparticles was synthesized through reduction reaction of $PtCl_6^{2-}$ solution using $NaBH_4$ with citric acid as the capping agent. Particles size between 4.46 to 4.78 nm were observed by using TEM measurements. The BDD microelectrodes were utilized to investigate the relationship between Pt nanoparticle size distribution and the current generated from the oxidation reaction of 15 mM hydrazine in a 50 mM phosphate buffer solution pH 7.4 in the presence of 1.0 mL nanoparticle solutions. A current range of 5 and 6 nA with a noise level of 0.15 nA was observed showing a good correlation with the particle sizes of Pt NPs. Comparison was also performed with the measurements using Au microelectrodes, indicated that the prepared BDD microelectrodes is promising for the measurements of nanoparticle sizes distribution, especially Pt NPs.
Keywords: boron-doped diamond (BDD); chronoamperometry; microelectrodes; platinum nanoparticles; size distribution

Cite This Article:
Aliyah, Nurhidayat, R. R., Sanjaya, A. R., Wibowo, R., Einaga, Y., Saepudin, E., & Ivandini, T. A. (2023). Preparation Of Boron-Doped Diamond Microelectrodes To Determine The Distribution Size Of Platinum Nanoparticles Using Current Transient Method. *Environmental and Materials, 1*(1), 8-19. https://doi.org/10.61511/eam.v1i1.2023.117

1. Introduction

Nanotechnology has emerged as a prominent field of study in science and engineering, captivating great attention in recent years. A pivotal moment in the history of nanotechnology can be traced back to Richard Feynman's influential lecture titled "There is Plenty Room at the Bottom," delivered in 1959. In this lecture, Feynman emphasized the vast potential of working at the micro- or nanoscale and addressed the challenges associated with manipulating and controlling matter on a small scale (Kuhlbusch et al., 2011). Since then, the utilization of nanoparticles has gained considerable popularity. Nanoparticles (NPs) are characterized as particles that are either dispersed or solid and possess sizes ranging from approximately 10 to 100 nm (Kuhlbusch et al., 2004). Owing to their small dimensions, nanoparticles demonstrate distinctive physical and chemical properties, making them highly desirable for a wide range of applications in scientific and

engineering disciplines(Jamkhande et al., 2019; Ndolomingo et al., 2020; Xia et al., 2013). To achieve a comprehensive understanding of their fundamental properties and optimize their performance for various applications, it is crucial to accurately characterize nanoparticles in terms of size, shape, and composition. Currently, methods like transmission electron microscopy (TEM), scanning electron microscopy (SEM), and particle size analyzers (PSA) are commonly used for nanoparticle size characterization (Wei et al., 2023). However, these techniques are expensive and require extensive maintenance (Navalón & García, 2016). Therefore, there is a need to develop new, affordable methods for nanoparticle size characterization that are easy to use and provide quick results.

Several electrochemical approaches for detecting single NPs by measuring their impact with the conducting surface of the microelectrode have been extensively investigated (Qiu et al., 2022; Sardesai et al., 2013; Zhou et al., 2012). For instance, in a significant study by Xiao et al. (2008) was found that the collision of single Pt NPs with the surface of the electrode could be observed by amplifying the electrocatalytic oxidation of hydrazine (Castañeda et al., 2015). Furthermore, the kinetic reactions on platinum, carbon, and gold electrodes exhibited distinct characteristics. A distinct profile of current versus time, representing the interaction between Pt NPs and the microelectrode surface, was observed (Fig. 1). Upon contact with the electrode, electrons flowed into or out of the nanoparticles, sustaining catalytic reactions on its surface. Consequently, these particle collisions produced individual current steps. The amplitude of these current steps, which occurred at the mass transfer limiting current, was determined by the following equation:

$$I = 4\pi(\ln 2)\ln FDCr \qquad (1)$$

where D represents the diffusion coefficient of reactants at concentration C, and r corresponds to the radius of a single nanoparticle (Dery et al., 2023). Therefore, the amplitude of each current step is directly correlated to the size of the nanoparticle (Kellon et al., 2019). By plotting the current amplitudes against the frequency of peak occurrence, a strong correlation was observed with the particle size distribution as determined by TEM. This electrochemical approach offers a rapid screening method for nanoparticle dispersions (Kellon et al., 2019; Suzuki et al., 2007).

Metal electrodes are known to have limitations, including susceptibility to oxidation, high background current, and significant noise during measurements. To address these challenges, boron-doped diamond (BDD) electrodes have been developed for electrochemical sensors. BDD electrodes offer several advantages, such as low charging current, chemical inertness, mechanical durability, a wide potential window, and low background current(Asai et al., 2016; Ivandini & Einaga, 2013; Ivandini et al., 2015; Muharam et al., 2019; Pino et al., 2015; Suzuki et al., 2007). Given these favorable properties, BDD electrodes hold great capability for effectively assessing the size distribution of Pt NPs. In this study, we propose a simple electrochemical method using BDD microelectrode in comparison with Au and Pt microelectrode to accurately determine the size of single nanoparticles.

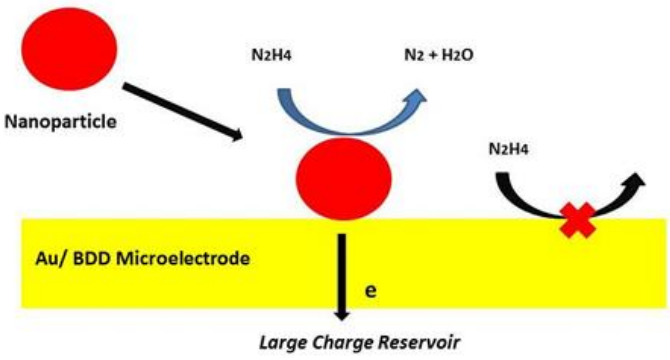

Figure 1. Illustration of nanoparticle collision on the microelectrode surface

2. Methods

2. Experimental Section

2.1. Chemicals

All chemicals were in analytical grade and used without further purification. Hexachloroplatinic acid hexahydrate ($H_2PtCl_6.6H_2O$, Pt 37.5%), chloroauric acid tetrahydrate ($HAuCl_4.4H_2O$), trisodium citrate dihydrate ($Na_3C_6H_5O_7.2H_2O$, 99%), sodium borohydride ($NaBH_4$, ≥98%), dipotassium hydrogen phosphate (K_2HPO_4), potassium dihydrogen phosphate (KH_2PO_4), hydrazine ($N_2H_4{\cdot}H_2O$, 64-65%), methanol, acetone, trimethoxyborane, epoxide, and 2-propanol were purchased from WAKO. Nanodiamond was obtained from Kemet Co. and all substance was diluted using double-distilled water produced by Millipore Direct-Q® 5 UV.

2.2. Fabrication of The Microelectrodes

The BDD microelectrode was prepared using tungsten needles (20 μm diameter). The needles were initially seeded by ultrasonicated in a suspension of nanodiamond particles in 2-propanol for 1.5 h. Then, the polycrystalline BDD particles was deposited onto the needle's surface using microwave plasma-assisted chemical vapor deposition (MPACVD) (ASTeX Corp.) with a plasma power of 2500 W for 10 h. A mixture of acetone and trimethoxyborane in a 50 : 4 (v/v) ratio was used as the precursor solution. The BDD microelectrode was insulated by filling a pre-pulled glass capillary (Narishige, Tokyo, Japan) and packed with epoxy. The film quality of the electrodes was assessed using Raman spectroscopy (Renishaw System 2000), while the surface termination was examined using XPS (Thermo Fisher Scientific Co.). The surface morphology of the electrode was investigated using a scanning electron microscope (SEM, JEOL JSM 5400). The resulting microelectrodes were then insulated by filling fine tip pipet tips with epoxy and incubating them at 60 ˚C overnight. Meanwhile, Au and Pt microelectrodes were fabricated by twisting Au wire (25 μm, Nilaco Corp.) and Pt wire (20 μm, Nilaco Corp.) into Cu wire using carbon tape.

2.3. Preparation of Pt Nanoparticles

The Pt nanoparticles (Pt NPs) solutions were prepared by reducing H_2PtCl_6 (2 mM) using sodium borohydride ($NaBH_4$) in the presence of sodium citrate. Specifically, 15 mL of 2 mM H_2PtCl_6 was mixed with 0.75 mL of 50 mM $Na_3C_6H_5O_7$, followed by the dropwise addition of 0.3 mL of fresh 60 mM and 90 mM $NaBH_4$ under vigorous magnetic stirring for 30 min. The resulting nanoparticles were characterized using UV-Vis (Thermo Fisher Scientific 1510) and TEM-EDX (FEI Tecnai G2 SuperTwin).

2.4. Electrochemical Measurements

Electrochemical measurements were carried out using a potentiostat (ALS/HCH Instruments) with the cyclic voltammetry (CV) and chronoamperometry (CA) techniques. The measurements were performed in a three-electrode cell containing 25 mL of electrolyte. The reference electrode Ag/AgCl was used, and a Pt spiral served as the counter electrode. To minimize external interference, the electrochemical cell was operated within a specific potential range (0 until +1.3 V) for the faradaic reaction. The electrolyte solution consisted of 15 mM hydrazine on 50 mM phosphate buffer solution (PBS) pH 7.4. The CV method was utilized to identify the optimum potential oxidation of hydrazine, while the CA method was used to investigate the electrocatalytic current amplifications caused by the collision phenomenon of Pt-NPs at the microelectrode surface in the presence of hydrazine. The CA measurement was chosen due to its suitability for observing the Pt-NPs collision phenomenon, as it minimizes the interference from reduction processes compared to the CV method. For each measurement, a volume of 1.0 mL of Pt NPs was injected.

3. Results and Discussion

3.1. Characterization of the Microelectrodes

The Raman spectrum of the BDD microelectrode (Fig. 2a) exhibited a sharp peak at around 1300 cm^{-1} corresponds to the C-C sp^3 bond characteristic of diamond (Ivandini & Einaga, 2021; Watanabe et al., 2006). Additionally, peaks at 500 and 1200 cm^{-1}, attributed to the Fano effect. This phenomenon is caused by the intricate coupling between phonons and electrons and it is closely associated with the presence of boron doping (Ivandini et al., 2012; Suzuki et al., 2007). Notably, the absence of a peak at 1500 cm^{-1}, indicating neither graphite nor amorphous carbon structures are formed.

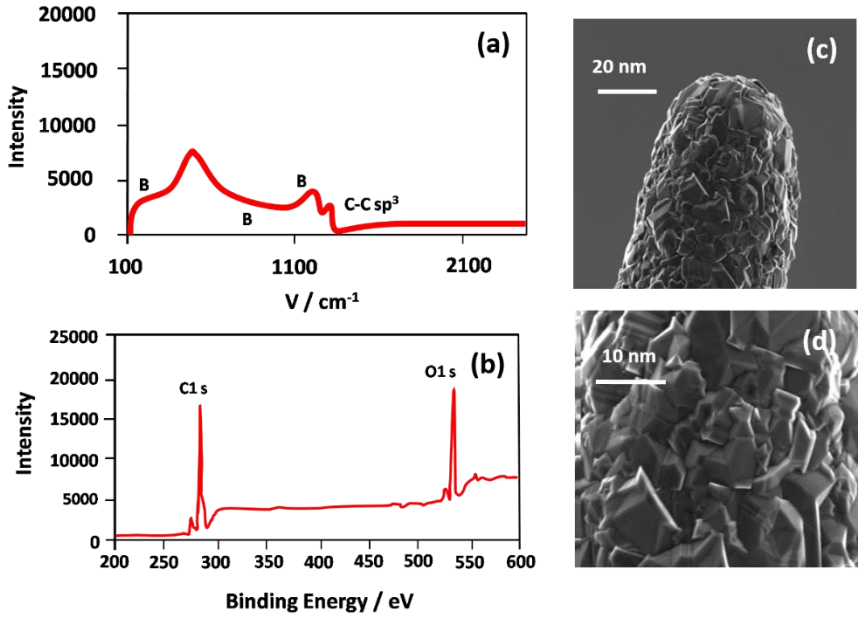

Figure 2. Typical Raman (a) and XPS (b) spectrum of BDD microelectrodes together with the related SEM Images in different magnifications (c-d)

The XPS spectrum of the BDD microelectrode (Fig. 2b) revealed a peak at 287.5 eV corresponding to C 1s. This peak is attributed to the presence of C-C and C-H bonds at the BDD terminal. The formation of C-H bonds can be attributed to the use of hydrogen gas as the carrier gas during the deposition process. Additionally, a peak at 532.9 eV was observed in the O 1s region, indicating the presence of C-O and O-H bonds. These bonds revealed that a portion of the C-H bonds has been replaced with C-O bonds, suggesting oxidation of the surface when exposed to the oxygen gas in the ambient air (Smith et al. 2016). The ratio of C 1s to O 1s was 6:5 calculated based on their respective peak intensities. The SEM analysis (Fig. 2c-d) at a magnification of 3500 times, shows the diameter of the electrode at around 25 µm, homogeneously covered with the diamond particles at around 5 µm size.

3.2. Characterization of Pt Nanoparticle

The H_2PtCl_6 solution exhibits a pale-yellow color prior to the reduction process and displays absorption at 265 nm in the UV-Vis spectrum, attributed to the ligand-to-metal charge-transfer transition of $[PtCl_6]^{2-}$ ions (Fig. 3a) (Jiang et al., 2011; Qiu et al., 2022). Following the reduction reaction by $NaBH_4$, the absorption peak at 265 nm vanishes, indicating the complete reduction of $[PtCl_6]^{2-}$ ions (Wu et al., 2014; You et al., 2017). Meanwhile, the color of the solution changes to a dark brown hue upon reduction process. The use of citrate ion as a capping agent was to facilitate the formation of stable Pt NPs in the colloidal solution. The presence of citrate is expected to initiate the Pt-O bonding and slowing the growth of particle, these coordination controlled makes the nanoparticle sizes by the position of citrate molecules (Jiang et al., 2011; Wu et al., 2014; You et al., 2017)

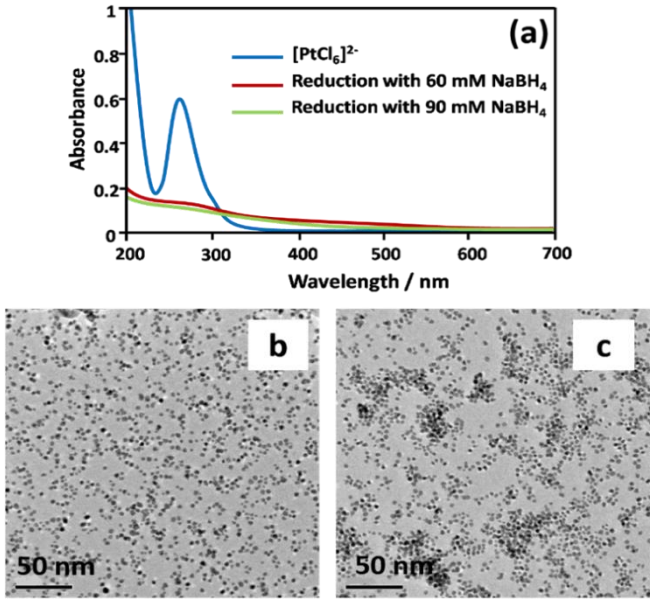

Figure 3. UV-Vis spectrum of Pt nanoparticle (a), TEM Images of Pt Nps produced from the reduction reaction using $NaBH_4$ at the concentrations of 60 mM (b) and 90 mM (c)

Characterization of the synthesized of Pt NPs using TEM-EDX depicted in Figs. 3b-c illustrate the formation of Pt NPs from the H_2PtCl_6 solution with sizes ranging from approximately 1 to 9 nm. Different concentrations of $NaBH_4$ were used. Interestingly, the distribution of Pt NPs sizes using either 60 mM or 90 mM $NaBH_4$ was found to be similar. The average diameter of Pt NPs produced from 60 mM $NaBH_4$ was approximately 4.78 nm, while with 90 mM $NaBH_4$ it was approximately 4.46 nm. It was observed that increasing the $NaBH_4$ concentration initiated the agglomeration process (Fig. 3c), despite the similarity in the major particle size compared to the lower $NaBH_4$ concentration. This phenomenon occurred due to the insufficient stabilization of the aggregate initiation by citric acid, which acted as a capping agent during the nanoparticle formation (Xiao & Bard, 2007).

The nanoparticle concentration is typically calculated based on the Pt precursor concentration divided by the average number of Pt atoms within each particle (Xiao et al., 2008; Xiao & Bard, 2007; Xu et al., 2019). Assuming an average diameter of 4.46 nm, the Pt NPs were estimated to contain 1734 atoms, resulting in a concentration of approximately 1.153 µM. Similarly, assuming an average diameter of about 4.78 nm, the Pt NPs were estimated to contain 1859 atoms, with a concentration of approximately 1.08 µM. These colloidal Pt NPs were employed for screening the size distribution of nanoparticles using an electrochemical method. These data confirmed the using of higher concentration of reducing agent will produce more particle on the nanoparticle formation process.

3.3. Screening Pt nanoparticle size distribution by using microelectrodes

CV was utilized to investigate the potential oxidation of Pt NPs and to determine the optimal potential window for observing collision events of single Pt NPs. The CV measurement was performed at Pt, Au, and BDD microelectrodes in the presence and absence of hydrazine, focusing on their electrocatalytic abilities. Fig. 4a illustrates the expected steady-state response of three different microelectrodes in a PBS electrolyte in the absence of hydrazine, which significantly differs in the presence of hydrazine (Fig. 4b). Particularly, the BDD microelectrodes show very low current levels, possibly due to the slower kinetics of the BDD material (Ivandini et al., 2012; Suzuki et al., 2007). Moreover, CV measurements of the BDD microelectrode indicated a narrower potential window compared to the other electrodes. This could be attributed to the presence of sp^2 carbon, suggesting that the increased sp^2 bond content limits the potential range of BDD electrodes. However, these conditions did not significantly affect the background current response depicted in Figure

4. In fact, the BDD electrode exhibited a lower background current compared to the Pt and Au electrodes (Xu & Einaga, 2020).

Furthermore, no peak was observed in the voltammograms of BDD (red line) in the presence of hydrazine. However, the voltammogram with the addition of hydrazine exhibited an oxidation peak at around +0.4 V and +0.8 V at Pt microelectrodes (black line), while a peak at around +0.4 V and +0.9 V was observed at the Au microelectrode (blue line). The peak at +0.9 V is not related to gold oxidation (Aliyah et al., 2022). Therefore, the peak at +0.4 V was confirmed to oxidation reaction of hydrazine into N_2 and H^+ at neutral pH at both Pt and Au microelectrodes. The results also confirmed the superiority of Pt microelectrode (represented by black lines) for the hydrazine oxidation reaction compared to Au and BDD microelectrodes (Miao & Compton, 2021). Based on the results, the potential of +0.4 V was selected to study the correlation between the current transient of Pt NPs due to hydrazine oxidation with the size distribution of the prepared nanoparticles using chronoamperometry on Au and BDD microelectrodes, taking advantage of the collision and adhesion of Pt NPs to the microelectrode surface (Jung et al., 2019). It was expected that this effect is likely acted to contribute in the electrocatalytic oxidation of hydrazine at the microelectrodes (Jung et al., 2019; Wei et al., 2023).

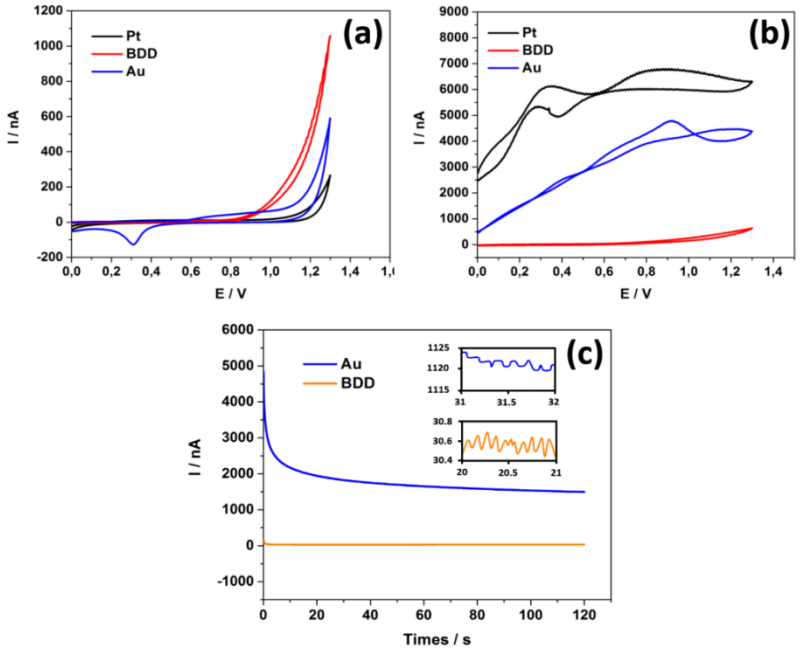

Figure 4. Voltammograms of 50 mM PBS solution using Au, BDD and Pt microelectrodes in the absence (a) and in the presence (b) of 15 mM hydrazine, and their related chronoamperograms (c) at a potential applied of +0.4 V (vs. Ag/AgCl). Interval sampling of 25 ms with the measurements time of 120 s was used. Inset in (c) magnifying the amperometric noises generated at Au and BDD microelectrode due to the collision of Pt Nps at the surface of microelectrodes

Chronoamperometry was performed by immersing each microelectrode in a 25 mL solution of hydrazine (15 mM) in PBS (50 mM) pH 7.4 to investigate the noise of hydrazine oxidation currents. The amperomograms show that the noise level of the BDD microelectrode was approximately 0.15 nA that siginificantly lower compared to the Au microelectrode at around 1 nA. The lower current response of the BDD microelectrode in the presence of hydrazine is related to the semiconductor properties of the BDD material, in which the diamond crystal structure provides excellent stability and minimizes noise during electrochemical reactions. This characteristic results in a lower background current for the BDD microelectrode, making it advantageous for electrochemical analysis (Ivandini et al., 2006, 2012; Suzuki et al., 2007).

The chronoamperometry measurements at BDD and Au microelectrode were then conducted in the presence of hydrazine in 50 mM PBS with and without Pt NPs (Fig. 5). A 1

mL sample of Pt NPs, produced through the reduction of 60 mM $NaBH_4$, was injected into the electrochemical cell, and the measurement was carried out for approximately 2 min. To clearly observe the amplitude of the current steps, the chronoamperogram was zoomed in every 5 s for 20 s duration. It should be noted that the large noise observed during the first 20 s of the measurement was caused by the opening and closing of the Faraday cage door while the Pt NPs solution was injected. After this period, the current experienced a slight offset, possibly due to one or a few particle collisions during that time period. Consequently, the current transient was monitored after the initial 20 s to distinguish the noise resulting from the injection and the closing of the Faraday cage (Alligrant et al., 2013; Xiao & Bard, 2007; Xu et al., 2019). In conclusion from Fig. 5, the chronoamperogram at both BDD and Au microelectrodes (Fig. 5(a) and (b), respectively) revealed the absence of any current transients. Thus, in the absence of an oxidizing agent, the amplitude of the current steps cannot be catalyzed on the surface of the microelectrode.

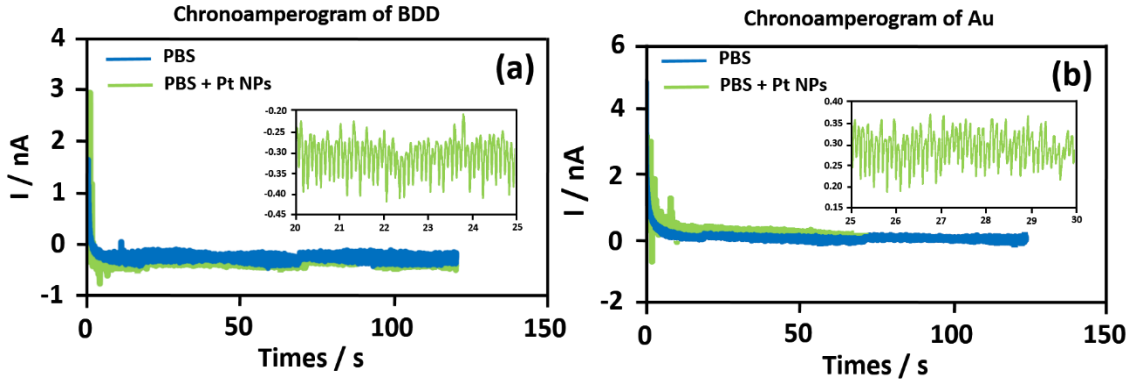

Figure 5. Chronoamperogram of 50 mM PBS with the addition of 1.0 mL colloidal Pt NPs produced by the reduction 60 mM $NaBH_4$ using BDD (a) and Au (b) microelectrode

Furthermore, the correlation between the oxidation current of hydrazine in the presence of Pt NPs at the and their size distribution (as determined by TEM) was studied at BDD microelectrode in comparison with at Au microelectrode. Two types of the colloidal nanoparticles, synthesized by 60 mM and 90 mM $NaBH_4$, were utilized for the measurements. The chronoamperometry results demonstrated an increase interval current when using the microelectrodes (Fig. 6). In contrast to the measurements conducted in the absence of hydrazine, the chronoamperogram in 50 mM PBS pH 7.4 in the presence of 15 mM hydrazine exhibited current transients that exceeded the noise level of the microelectrode.

The chronoamperogram obtained using the BDD microelectrode exhibited the increase of current transients (Fig. 6a-c), depicting the current transients during the measurement of 1.0 mL of Pt NPs synthesized using 60 mM $NaBH_4$. These current transients range from 3 to 18 nA within that time interval, surpassing the noise level of the BDD microelectrode at 0.15 nA. Meanwhile, Fig. 6(d) illustrates the current transients observed using an Au microelectrode. The current transients at 65 - 70 s range from 4 to 24 nA Fig. 6(e,f), surpassing the noise levels of the Au microelectrode at 1.0 nA. These current transients can be attributed to the oxidation reaction of hydrazine in the presence of Pt NPs. Comparison between BDD and Au microelectrodes showed that the utilization of carbon-based material in the BDD microelectrode contributed to a lower current transient response, allowing the greater stability in the oxidation reaction of hydrazine. The application of the BDD microelectrode exhibited not only lower current transients but also reduced the noise responses, resulted from the less adsorption properties of the sp^3 bonding. This result indicated that the proposed electrodes is promising for accurately measuring the size distribution of nanoparticle species.

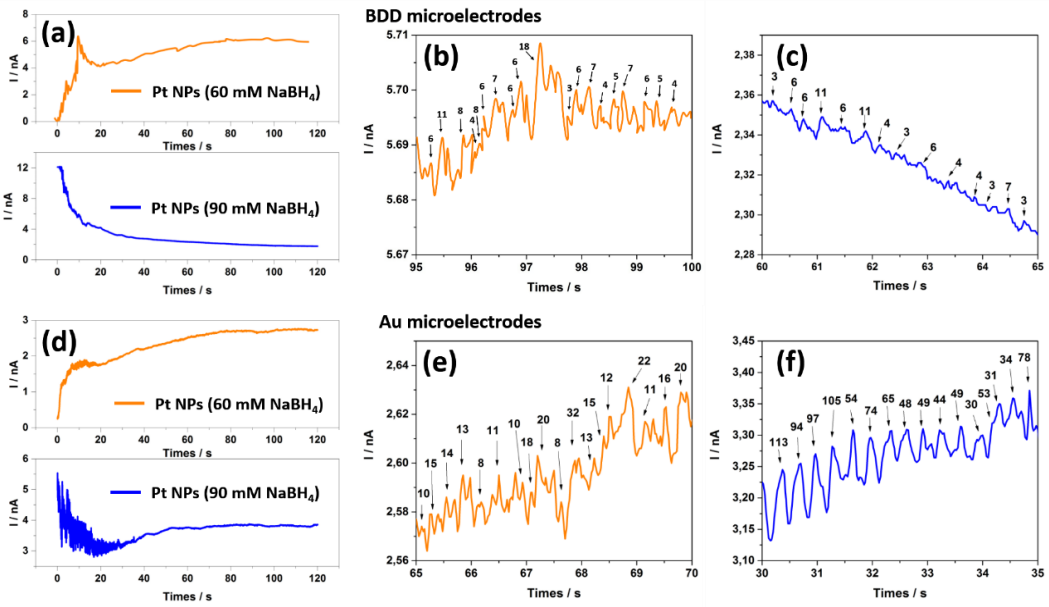

Figure 6. Chronoamperogram of 50 mM PBS containing hydrazine in the presence of 1.0 mL colloidal Pt NPs solution synthesized by reduction reaction with 60 mM and 90 mM $NaBH_4$, measured using BDD (a, b, c) and Au microelectrode (d, e, f) in the certain interval time

Furthermore, the current transients obtained during the measurements using both the gold and BDD microelectrodes were compared with the size distribution results obtained from TEM. It was observed that the sizes of the nanoparticles predominantly present in the colloidal solution often collided with the microelectrode surface, resulting in the occurrence of current transients during the measurements. The current transients primarily appeared in good correlation with the sizes of the nanoparticles that were most frequently observed in the TEM distribution results.

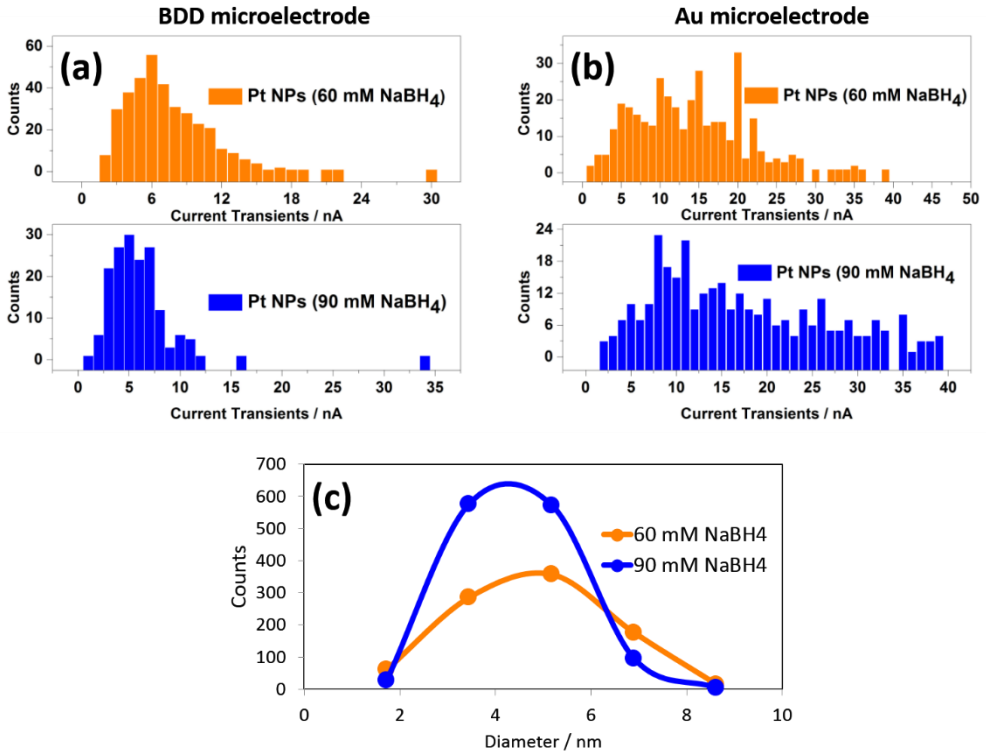

Figure 7. Distributions of the current transients generated in chromatogram in Fig. 6 at BDD microelectrode (a), using Au microelectrode (b), and the size distribution by TEM (c)

The chronoamperometry of 1.0 mL of colloidal Pt NPs produced from 60 mM $NaBH_4$ using the BDD microelectrode observed the current transients at around 6 nA as shown in the plots in Fig. 7a (orange chart), while the measurements using Au microelectrode generated the current transient in approximately of 20 nA (Fig.7b orangechart). Comparing these results with the size distribution obtained from TEM (Fig. 7c), it can be inferred that the current transient of 20 nA from the gold microelectrode and 6 nA obtained from BDD microelectrode reflects nanoparticles with an average size of 5.17 nm. Meanwhile, TEM images of the Pt NPs colloidal nanoparticles solution produced from 90 mM $NaBH_4$ showed that nanoparticles with an average size of 3.45 nm were frequently observed. Correspondingly, the frequently observed current transients in this colloidal solution were approximately 5 nA with the BDD microelectrode (Fig. 7a, blue chart) and 8 nA with the gold microelectrode (Fig. 7(b), bluechart). Therefore, it can be assumed that the both current transients reflect nanoparticles with an average size of 3.45 nm. As previously mentioned, according to the Equation 1, there is a decrease in nanoparticle size results in a lower current response. These phenomena proclaim that the suitable performance of BDD microelectrode compared to the Au microelectrode as screening distribution size of nanoparticle. The origin catalytic performance of BDD was promising which demonstrated by the current transient response of BDD electrode is much lower than the Au microelectrode and also followed by smaller noise current response.

4. Conclusions

In conclusion, BDD polycrystalline was successfully synthesized at a tungsten wire using microwave plasma-assisted chemical vapor deposition methods. The microelectrode with the diameters of 25 μm could be prepared with an average partiile size of 25 μm. Meanwhile, Pt NPs synthesized through the reduction reaction using $NaBH_4$ with citric acid as the capping agent produced nanoparticles with an approximately sizes of 4.78 nm and 4.46 nm with the Pt concentrations of 1.076 μM and 1.153 μM, respectively. The use of the BDD microelectrodes for hydrazine oxidation in the presences of 1.0 mL solution of the prepared nanoparticles Pt, exhibited an average transient current response of 5 and 6 nA, respectively, while the measurements using Au microelectrodes conducted for the comparison showed the transient currents of 11 and 20 nA, respectively. Overall, the experiments concluded that the BDD microelectrodes, with its stable current transients and lower noises of current response, was good suited to the TEM results of Pt NPs. The results indicate that the prepared BDD microelectrode is promising for screening the size distribution of nanoparticles.

Acknowledgement

We would like to thank the Ministry of High Technology and Education Indonesia for Hibah PUPT Dikti 2021.

Author Contribution

RRN, ES YE, and ITA: Conceptualization, data curation, formal analysis, and writing the original draft. AA and ARS : Analysis, validation, writing – review and editing. ES and ITA : Data curation and formal analysis. ES, EY, and ITA: validation, funding acquisition, and supervisor.

Funding

The work was supported by NKB-169/UN2.RST/HKP.05.00/2021.

Informed Consent Statement

Informed consent was obtained from all subjects involved in the study.

Data Availability Statement

All research data are available.

Conflicts of Interest

The authors declare no conflict of interest.

Reference

Aliyah, Nasution, M. A. F., Putri, Y. M. T. A., Gunlazuardi, J., and Ivandini, T. A., (2022.) Modification of Carbon Foam with 4-Mercaptobenzoic Acid Functionalised Gold Nanoparticles for an Application in a Yeast-Based Microbial Fuel Cell. *RSC Advances* 12 (44), 28647-57. https://doi.org/10.1039/d2ra05100a

Alligrant, T. M., Nettleton, E. G., & Crooks, R. M. (2013). Electrochemical detection of individual DNA hybridization events. *Lab Chip*, *13*(3), 349-354. https://doi.org/10.1039/C2LC40993C

Asai, K., Ivandini, T. A., Falah, M., & Einaga, Y. (2016). Surface termination effect of boron-doped diamond on the electrochemical oxidation of adenosine phosphate. *Electroanalysis 128*(1), 177-182. https://doi.org/10.1002/elan.201500505

Castañeda, A. D., Alligrant, T. M., Loussaert, J. A., & Crooks, R. M. (2015). Electrocatalytic Amplification of Nanoparticle Collisions at Electrodes Modified with Polyelectrolyte Multilayer Films. *Langmuir*, *31*(2), 876-885. https://doi.org/10.1021/la5043124

Dery, L., Dery, S., Gross, E., & Mandler, D. (2023). Influence of Charged Self-Assembled Monolayers on Single Nanoparticle Collision. *Analytical Chemistry*, *95*(5), 2789-2795. https://doi.org/10.1021/acs.analchem.2c04081

Ivandini, T. A., Rao, T. N., Fujishima, A., & Einaga, Y. (2006). Electrochemical oxidation of oxalic acid at highly boron-doped diamond electrodes. *Analytical chemistry*, *78*(10), 3467-3471. https://doi.org/10.1021/ac052029x

Ivandini, T. A., Saepudin, E., Wardah, H., Harmesa, Dewangga, N., & Einaga, Y. (2012). Development of a biochemical oxygen demand sensor using gold-modified boron doped diamond electrodes. *Analytical chemistry*, *84*(22), 9825-9832. https://doi.org/10.1021/ac302090y.

Ivandini, T. A. & Einaga, Y. (2013). Electrochemical detection of selenium (IV) and (VI) at gold-modified diamond electrodes. *Electrocatalysis*, *4*, 367-374. https://doi.org/10.1007/s12678-013-0169-7

Ivandini, T. A. & Einaga, Y. (2021). Electrochemical Sensing Applications Using Diamond Microelectrodes. *Bulletin of Chemical Society of Japan*, *94*, 2838-2847. https://doi.org/10.1246/bcsj.20210296

Ivandini, T. A., Saepudin, E. & Einaga, Y. (2015). Yeast-based biochemical oxygen demand sensors using Gold-modified boron-doped diamond electrodes. *Analytical Sciences*, *31*(7), 643-649. https://doi.org/10.2116/analsci.31.643

Jamkhande, P. G., Ghule, N. W., Bamer, A. H., & Kalaskar, M. G. (2019). Metal nanoparticles synthesis: An overview on methods of preparation, advantages and disadvantages, and applications. *Journal of Drug Delivery Science and Technology*, *53*, 101174. https://doi.org/10.1016/j.jddst.2019.101174

Jiang, Q., Peng, Z., Xie, X., Du, K., Hu, G., & Liu, Y. (2011). Preparation of high active Pt/C cathode electrocatalyst for direct methanol fuel cell by citrate-stabilized method. *Transactions of Nonferrous Metals Society of China*, *21*(1), 127-132. https://doi.org/10.1016/S1003-6326(11)60688-2

Jung, Y., Ju, I. G., Choe, Y. H., Kim, Y., Park, S., Hyun, Y.-M., Oh, M. S., & Kim, D. (2019). Hydrazine Exposé: The Next-Generation Fluorescent Probe. *ACS Sensors*, *4*(2), 441-449. https://doi.org/10.1021/acssensors.8b01429

Kellon, J. E., Young, S. L., & Hutchison, J. E. (2019). Engineering the Nanoparticle–Electrode Interface. *Chemistry of Materials*, *31*(8), 2685-2701. https://doi.org/10.1021/acs.chemmater.8b04977

Kuhlbusch, T. A., Asbach, C., Fissan, H., Göhler, D., & Stintz, M. (2011). Nanoparticle exposure at nanotechnology workplaces: A review. *Particle and Fibre Toxicology*, *8*(1), 22. https://doi.org/10.1186/1743-8977-8-22

Kuhlbusch, T. A. J., Neumann, S., & Fissan, H. (2004). Number Size Distribution, Mass Concentration, and Particle Composition of PM_{1}, $PM_{2.5}$, and PM_{10} in Bag Filling Areas

of Carbon Black Production. *Journal of Occupational and Environmental Hygiene*, *1*(10), 660-671. https://doi.org/10.1080/15459620490502242

Miao, R. & Compton, R. G. (2021). The electro-oxidation of hydrazine: a self-inhibiting reaction. *The Journal of Physical Chemistry Letters*, *12*(6), 1601-1605. https://doi.org/10.1021/acs.jpclett.1c00070

Muharam, S., Jiwanti, P. K., Gunlazuardi, J., Einaga, Y., & Ivandini, T. A. (2019). Electrochemical oxidation of palmitic acid solution using boron-doped diamond electrodes. *Diamond and Related Materials*, *99*, 107464. https://doi.org/10.1016/j.diamond.2019.107464.

Navalón, S. & García, H. (2016). Nanoparticles for Catalysis. *Nanomaterials*, *6*(7), 123. https://doi.org/10.3390/nano6070123

Ndolomingo, M. J., Bingwa, N., & Meijboom, R. (2020). Review of supported metal nanoparticles: synthesis methodologies, advantages and application as catalysts. *Journal of Materials Science*, *55*(15), 6195-6241. https://doi.org/10.1007/s10853-020-04415-x

Pino, F., Ivandini, T. A., Nakata, K., Fujishima, A., Merkoçi, A., Einaga, Y. (2015). Magnetic enzymatic platform for organophosphate pesticide detection using boron-doped diamond electrodes. *Analytical Sciences*, *31*(10), 1061-1068. https://doi.org/10.2116/analsci.31.1061

Qiu, X., Tang, H., Dong, J., Wang, C., & Li, Y. (2022). Stochastic Collision Electrochemistry from Single Pt Nanoparticles: Electrocatalytic Amplification and MicroRNA Sensing. *Analytical Chemistry*, *94*(23), 8202-8208. https://doi.org/10.1021/acs.analchem.2c00116

Sardesai, N. P., Andreescu, D., & Andreescu, S. (2013). Electroanalytical Evaluation of Antioxidant Activity of Cerium Oxide Nanoparticles by Nanoparticle Collisions at Microelectrodes. *Journal of the American Chemical Society*, *135*(45), 16770-16773. https://doi.org/10.1021/ja408087s

Smith, M., Scudiero, L., Espinal, J., McEwen, J. S., & Garcia-Perez, M. (2016). *Improving the Deconvolution and Interpretation of XPS Spectra from Chars by Ab Initio Calculations*. *Carbon*. Vol. 110. Elsevier Ltd. https://doi.org/10.1016/j.carbon.2016.09.012

Suzuki, A., Ivandini, T. A., Yoshimi, K., Fujishima, A., Oyama, G., Nakazato, T., ... & Einaga, Y. (2007). Fabrication, Characterization, and Application of Boron-Doped Diamond Microelectrodes for in Vivo Dopamine Detection. *Analytical Chemistry*, *79*(22), 8608-8615. https://doi.org/10.1021/ac071519h

Watanabe, T., Ivandini, T. A., Makide, Y., Fujishima, A., & Einaga, Y. (2006). Selective detection method derived from a controlled diffusion process at metal-modified diamond electrodes. *Analytical chemistry*, *78*(22), 7857-7860. https://doi.org/10.1021/ac060860j.

Wei, W., Gou, R., Shu, C., & Guo, Z. (2023). Revealing Controlled Etching Behaviors of Gold Nanobipyramids by Carbon Film Liquid Cell Transmission Electron Microscopy. *The Journal of Physical Chemistry C*, *127*(16), 7808–7815. https://doi.org/10.1021/acs.jpcc.2c08530

Wu, G.-W., He, S.-B., Peng, H.-P., Deng, H.-H., Liu, A.-L., Lin, X.-H., Xia, X.-H., & Chen, W. (2014). Citrate-Capped Platinum Nanoparticle as a Smart Probe for Ultrasensitive Mercury Sensing. *Analytical Chemistry*, *86*(21), 10955-10960. https://doi.org/10.1021/ac503544w

Xia, Y., Yang, H., & Campbell, C. T. (2013). Nanoparticles for Catalysis. *Accounts of Chemical Research*, *46*(8), 1671-1672. https://doi.org/10.1021/ar400148q

Xiao, X. & Bard, A. J. (2007). Observing Single Nanoparticle Collisions at an Ultramicroelectrode by Electrocatalytic Amplification. *Journal of the American Chemical Society*, *129*(31), 9610-9612. https://doi.org/10.1021/ja072344w

Xiao, X., Fan, F.-R. F., Zhou, J., & Bard, A. J. (2008). Current Transients in Single Nanoparticle Collision Events. *Journal of the American Chemical Society*, *130*(49), 16669-16677. https://doi.org/10.1021/ja8051393

Xu, W., Zou, G., Hou, H., & Ji, X. (2019). Single Particle Electrochemistry of Collision. *Small*, *15*(32), 1804908. https://doi.org/10.1002/smll.201804908

Xu, J., & Einaga, Y. (2020). Effect of sp2 species in a boron-doped diamond electrode on the electrochemical reduction of CO_2. *Electrochemistry Communications*, *115*, 106731. https://doi.org/10.1016/j.elecom.2020.106731.

You, J.-G., Shanmugam, C., Liu, Y.-W., Yu, C.-J., & Tseng, W.-L. (2017). Boosting catalytic activity of metal nanoparticles for 4-nitrophenol reduction: Modification of metal naoparticles with poly(diallyldimethylammonium chloride). *Journal of Hazardous Materials*, *324*, 420-427. https://doi.org/10.1016/j.jhazmat.2016.11.007

Zhou, H., Park, J. H., Fan, F.-R. F., & Bard, A. J. (2012). Observation of Single Metal Nanoparticle Collisions by Open Circuit (Mixed) Potential Changes at an Ultramicroelectrode. *Journal of the American Chemical Society*, *134*(32), 13212-13215. https://doi.org/10.1021/ja305573g